Supporting Information

Polissar et al. 10.1073/pnas.1219681110

SI Text

SI Reconstructions of Continental Climate from the Cariaco Basin

The Cariaco Basin is a marginal tectonic basin located immediately north of the Cordillera de la Costa, Venezuela. Sediment records from this basin have been a cornerstone for arguments that climate is antiphased between the northern and southern hemispheres of South America on precession timescales.

Sediments in the basin alternate seasonally between a light-colored, biogenic, and carbonate-rich layer and a dark-colored, mineral-rich terrigenous layer (1). The light layers are generated during the northern hemisphere dry season (boreal winter) when strong trade winds induce upwelling of nutrient-rich waters that drive abundant marine algal production. Dark layers are generated during the terrestrial wet season when fluvial runoff delivers aluminosilicate-rich sediments and slackened trade winds reduce nutrient delivery and marine productivity. Proxies for terrigenous sediment concentration and sediment composition inferred from sediment color disagree on the direction and magnitude of climate changes during the Holocene (Fig. S1) (2–6). Cariaco Basin sediment trap studies indicate that terrigenous flux does not simply reflect coastal rainfall and that the better correlation between rainfall and terrigenous sediment concentration primarily reflects dilution from biogenic sediments (7). This and other studies suggest a more complicated control over terrigenous geochemical indicators in the Cariaco Basin record during the Holocene (8).

SI Study Site, Coring, and Chronology

Laguna Blanca [8.33°N, 71.78°W, 1,620 m above sea level (a.s.l.)] is a small (0.05 km^2), shallow (5.5 m deep) lake situated on the north slope of the Cordillera de Mérida in the Venezuelan Andes (Fig. S2). The lake water is acidic (pH = 5.9), highly dilute (58 $\mu S \cdot cm^{-1}$), and anoxic within 50 cm of the sediment–water interface (9). The bathymetry is a simple bowl with a single deep basin, no surface inflow, and a lake level currently 5 m below a conspicuous dry outflow channel. The 0.87 km^2 catchment is forested and contains an upstream dry lake that would drain into Laguna Blanca during wet intervals when sufficient precipitation is available. The watershed is situated in steep local topography above any regional aquifers, precluding regional groundwater input to the lake. There is no evidence of recent or past glaciation in the catchment, consistent with its location below both modern and Pleistocene glaciation limits (10, 11). Lake-water $\delta^{18}O$ and δD are enriched relative to modern precipitation and groundwater, and lie along an evaporation trend distinct from local and global meteoric water lines ($\delta^{18}O_{lake}$, –1.7 ‰; $\delta^{18}O_{precip}$, –7‰ Vienna Standard Mean Ocean Water) (9). Both the lack of surface outflow and enriched water isotopes indicate the lake is hydrologically closed and at present undergoes significant evaporative enrichment.

In 1999 we recovered overlapping sediment cores from the deepest part of Laguna Blanca using a square-rod coring system (12). Accelerator mass-spectrometry (AMS) radiocarbon dates on terrestrial macrofossils constrain the age–depth relationship for the cores. Radiocarbon ages were converted to calendar ages using the IntCal04 dataset (Table S1) (13, 14). The age model (Fig. S3) was constructed by linear interpolation between the calibrated ^{14}C ages.

The composite stratigraphy from Laguna Blanca is 482 cm long with sediments that vary from organic-rich to clastic-dominated. The base of the core dates to 11,000 cal·y before present (BP) and all radiocarbon ages are in stratigraphic order except the samples at 188.5 and 175 cm. The 175 cm age appears too old and is not included in the age model, because it produces an abrupt shift in sedimentation rates during a period in the core where the sediment lithology suggests low and constant sedimentation rates, with no evidence of an unconformity. The two deepest radiocarbon samples in the age model were measured on bulk sediment rather than terrestrial macrofossils and as such are considered maximum limiting ages (15).

The calibrated radiocarbon age from Laguna Brava (Table S1) is located immediately above a desiccation layer and dates the end of the desiccation event. This event has a correlative lithostratigraphic expression in the Laguna Blanca record.

SI Seasonal Insolation Forcing and Tropical Climate Evolution

It is possible that transition season insolation changes (Spring or Fall) could play a role in Venezuelan climate or elsewhere by altering precipitation during the early or late wet season in regions that express two wet seasons per year. However, this interpretation appears unlikely for two reasons. First, during the Holocene, decreased insolation in the northern hemisphere during March–April–May is balanced by increased insolation during September–October–November (Fig. S4) (16). Thus, any reduction in precipitation during the early part of the wet season would reasonably be balanced by an increase in the later part of the wet season. Second, insolation forcing during these transition seasons cannot explain the heterogeneous pattern of wet or dry changes that occur within the same hemisphere (and in some cases regionally). Thus, although transition season insolation is perhaps relevant to specific individual localities, it cannot explain the Holocene climate history at all of the sites in the same way as Pacific sea-surface temperature (SSTs).

SI Correlation of South American Precipitation with SSTs

Correlations of gridded precipitation products with various SST time-series were used to explore the influence of tropical Pacific, Atlantic, and Caribbean SSTs on South American climate. Mean annual SSTs from the Nino 3.4, Caribbean, north Atlantic, and south Atlantic regions (Fig. S5) were spatially correlated with South American rainfall from the University of Delaware gridded data product (17) (UDel precipitation v.2.01 provided by the National Oceanic and Atmospheric Administration's Earth System Research Laboratory, Physical Sciences Division, www.esrl.noaa.gov/psd/).

SI Influence of El Niño-Southern Oscillation Variability on South American Precipitation

The nonlinear response of precipitation to SST variability has a strong influence on precipitation in the Venezuelan and Bolivian Andes. In the Venezuelan and Bolivian Andes, cold SST events have larger precipitation anomalies compared with warm events (Fig. S6). This asymmetry means that SST variability (as opposed to the mean state) can significantly increase the long-term water budget of these regions due to the disproportionate precipitation increase during cold events. Thus, both the linear response to mean SST conditions and the nonlinear response to SST variability are important determinants of climate in these regions. Wetter conditions occur when eastern equatorial Pacific SSTs are reduced or SST variability increases.

SI Reconstructed Lake Level

Past lake levels were approximated by calculating leading principle components of sediment properties scaled to modern lake bathymetry. Principle component analysis (PCA) of sediment compositional parameters [loss-on-ignition, dry density, elemental carbon/nitrogen (C/N) ratios, and the mass accumulation rate of mineral sediments] yields a first axis that captures 76% of the variance and separates dense, rapidly accumulating, organic poor sediments from less dense, slowly accumulating, organic matter-rich sediments (Fig. S7). These differences reflect high and low lake levels, respectively. The middle lake depth of ~5 m corresponds to moderate bulk density, loss on ignition (LOI), C/N, and mass accumulation rates between 1,000–2,000 y BP (Fig. S8). The overflowing lake depth corresponds to the 10 m elevation of the spill point above the modern lake floor, as prescribed for the 0–500 and 9,000–11,000 y BP intervals. In this model, wetland deposits correspond to a water depth of ~1 m above the modern lake floor, represented by the 4,000–7,000 y BP interval.

1. Hughen KA, Overpeck JT, Peterson LC, Anderson RF (1996) The nature of varved sedimentation in the Cariaco Basin, Venezuela, and its palaeoclimatic significance. *Geol Soc Lond Spec Publ* 116(1):171–183.
2. Hughen KA, et al. (1998) Deglacial changes in ocean circulation from an extended radiocarbon calibration. *Nature* 391:65–68.
3. Hughen KA, Overpeck JT, Peterson LC, Trumbore S (1996) Rapid climate changes in the tropical Atlantic region during the last deglaciation. *Nature* 380:51–54.
4. Peterson LC, Haug GH, Hughen KA, Röhl U (2000) Rapid changes in the hydrologic cycle of the tropical Atlantic during the last glacial. *Science* 290(5498):1947–1951.
5. Haug GH, Hughen KA, Sigman DM, Peterson LC, Röhl U (2001) Southward migration of the intertropical convergence zone through the Holocene. *Science* 293(5533): 1304–1308.
6. Piper DZ, Dean WE, Jr. (2002) *Trace-Element Deposition in the Cariaco Basin, Venezuela Shelf, Under Sulfate-Reducing Conditions—A History of the Local Hydrography and Global Climate, 20 ka to the Present* (US Geological Survey, Denver, CO), pp 1–45.
7. Martinez NC, et al. (2007) Modern climate forcing of terrigenous deposition in the tropics (Cariaco Basin, Venezuela). *Earth Planet Sci Lett* 264(3-4):438.
8. Martinez NC, et al. (2010) Local and regional geochemical signatures of surface sediments from the Cariaco Basin and Orinoco Delta, Venezuela. *Geology* 38(2): 159–162, 10.1130/g30487.1.
9. Polissar PJ (2005) Lake records of Holocene climate change, Cordillera de Mérida, Venezuela. PhD dissertation (Univ of Massachusetts, Amherst, MA).
10. Schubert C (1974) Late Pleistocene Mérida Glaciation, Venezuelan Andes. *Boreas* 3(4): 147–151.
11. Stansell N, Polissar PJ, Abbott MB (2007) Last Glacial Maximum equilibrium-line altitude and paleo-temperature reconstructions for the Cordillera de Mérida, Venezuelan Andes. *Quaternary Research* 67:115–127, 110.1016/j.yqres.2006.1007.1005.
12. Wright HE, Mann DH, Glaser PH (1984) Piston corers for peat and lake sediments. *Ecology* 65:657–659.
13. Stuiver M, Reimer PJ, Braziunas TF (1998) High-precision radiocarbon age calibration for terrestrial and marine samples. *Radiocarbon* 40:1127–1151.
14. Reimer PJ, et al. (2004) IntCal04. *Radiocarbon* 46:1029–1058.
15. Abbott MB, Stafford TW (1996) Radiocarbon geochemistry of modern and ancient arctic lake systems, Baffin Island, Canada. *Quat Res* 45:300–311.
16. Berger A, Loutre MF (1991) Insolation values for the climate of the last 10 million years. *Quat Sci Rev* 10:297–317.
17. Legates DR, Willmott CJ (1990) Mean seasonal and spatial variability in gauge-corrected, global precipitation. *Int J Climatol* 10(2):111–127.

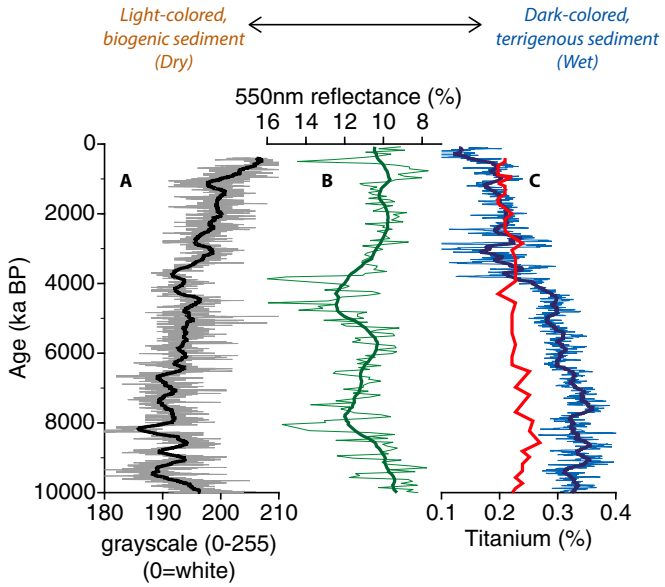

Fig. S1. Cariaco Basin sediment color and geochemistry. Grayscale (*A*, core PL07-56PC) (2, 3) and 550 nm reflectance (*B*, Ocean Drilling Program core ODP-1002C) (4) of Cariaco sediments indicates the contribution of light biogenic versus dark terrigenous sediment during the Holocene. Titanium concentrations measured by scanning X-ray fluorescence (*C*, blue line, core ODP-1002C) (5) and dissolution/inductively coupled plasma atomic emission spectroscopy (*C*, red line, core PL07-39PC) (6) reflect the concentration of terrigenous sediment. Disagreement between the reflectance records and the measured titanium concentrations suggests a more complicated proxy–climate relationship for these measurements than has been previously discussed.

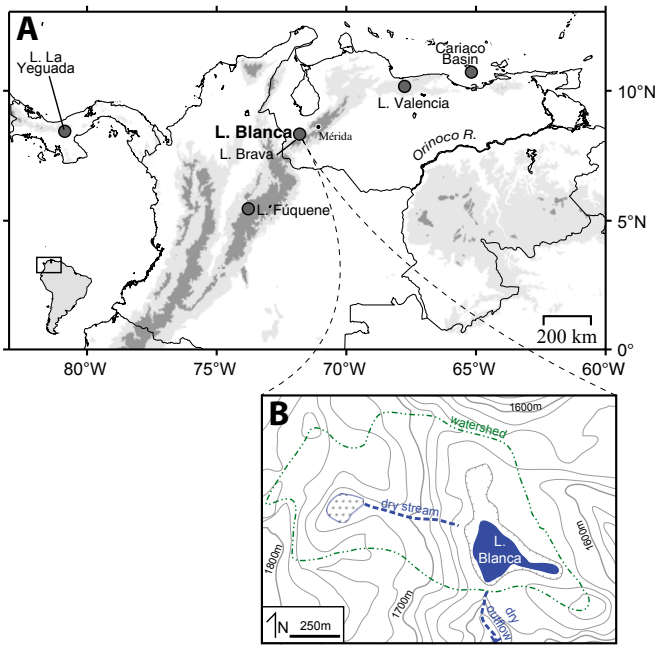

Fig. S2. Overview map showing Laguna Blanca and the location of other climate and paleoclimate records mentioned in the main text (*A*) and topography of the Laguna Blanca watershed (*B*). In *A*, Shading indicates elevations above 500 m (light gray) and 2000 m (dark gray).

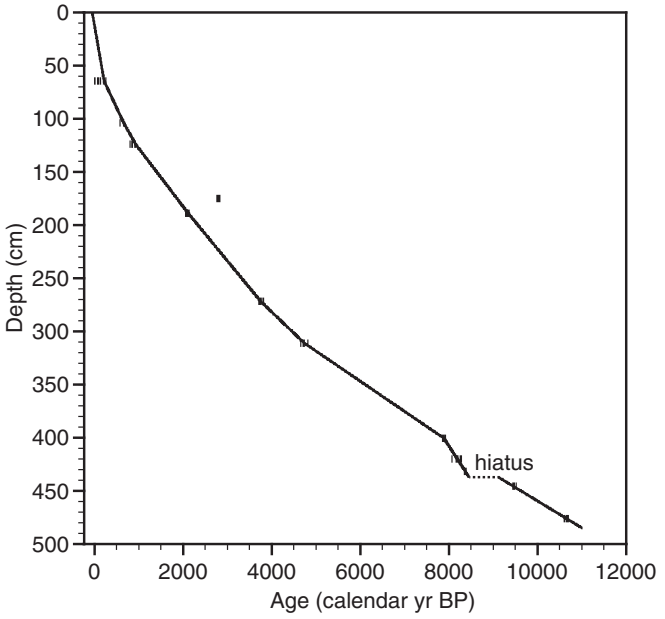

Fig. S3. Age–depth relationship for Laguna Blanca. The black bars indicate calibrated radiocarbon age ranges (1σ).

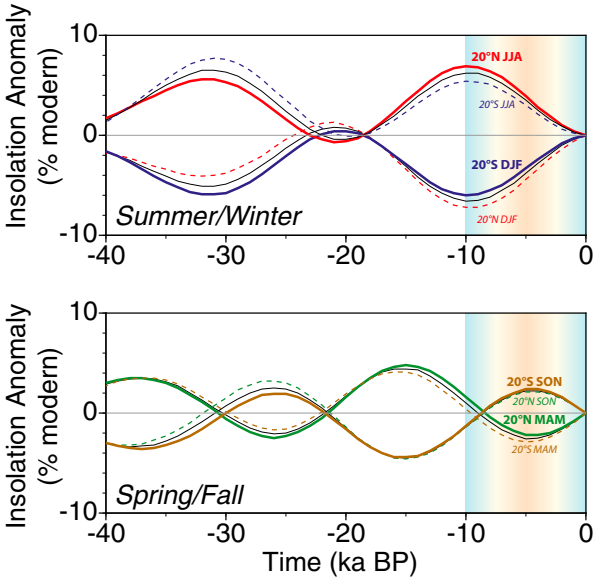

Fig. S4. Insolation anomalies for summer/winter and spring/fall (calculated from ref. 16).

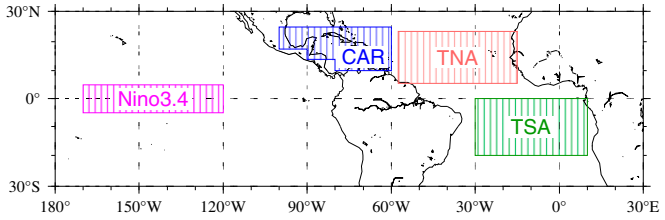

Fig. S5. Geographic regions defining the SST time-series.

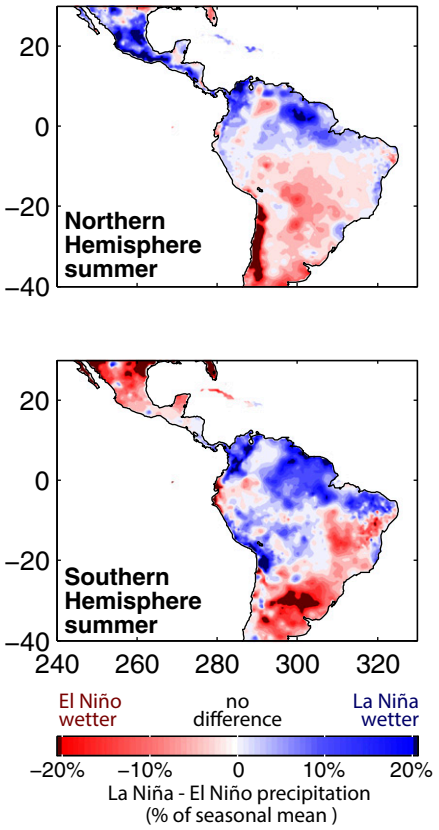

Fig. S6. Nonlinear impact of cold versus warm equatorial Pacific SSTs on South American precipitation. Shown is the wet season precipitation of the 10 coldest minus 10 warmest SST events between 1950–2000 A.D. as percentages of local mean wet-season precipitation. Strongly positive or negative anomalies (blue or red) indicate regions where El Niño-Southern Oscillation variability has a positive effect on local precipitation. In northern hemisphere summer (May–September), SST variability increases wet season precipitation in the Venezuelan Andes by almost 20%, whereas in southern hemisphere summer (November–March) precipitation in the region of Lake Titicaca increases by a corresponding amount. The October–December period of a 5-mo running average for Niño 3.4 SSTs was used to rank years. Precipitation anomalies from the University of Delaware Gridded Precipitation Product (v2.01) (17) are calculated for May–September of that year (northern hemisphere) and November–March of the following year (southern hemisphere).

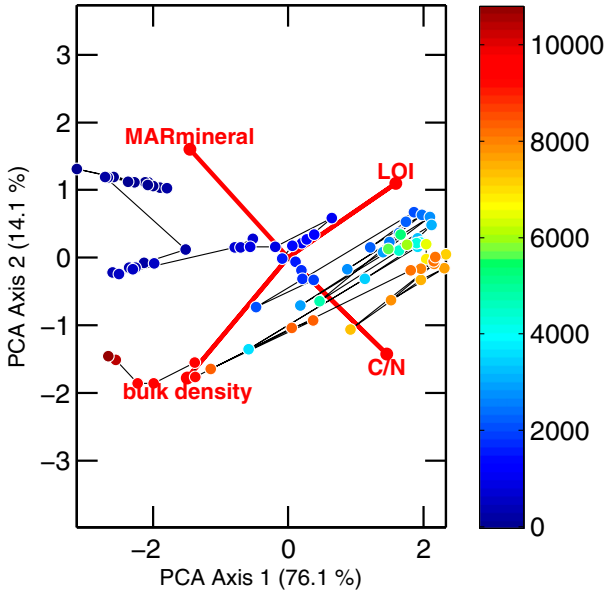

Fig. S7. PCA of sediment properties expressed as *z*-scores. Variable loadings are plotted with red lines and circles (3× magnitude for clarity), whereas sample scores are plotted with black lines and circles colored by sediment age. PCA axis 1 separates dense, high mineral mass accumulation rate sediments from those with high organic content and contributions from terrestrial organic matter.

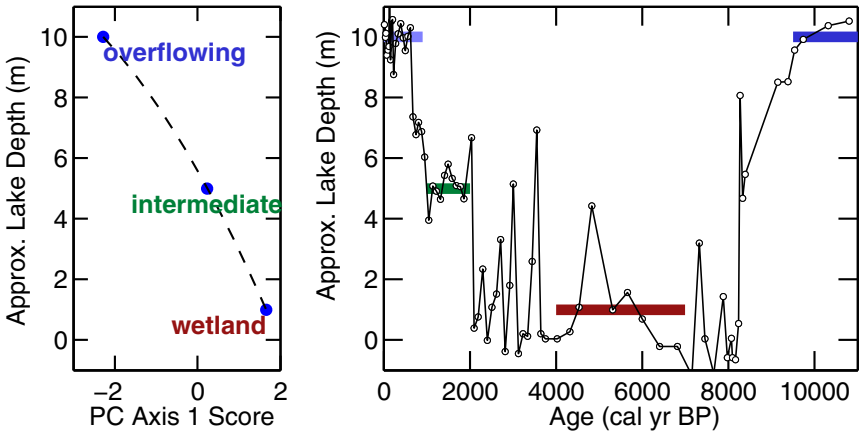

Fig. S8. PCA axis 1 scores were scaled to lake level (*Left*) based upon assumed intermediate lake levels 1,000–2,000 y BP, overflowing conditions during the early and late Holocene and low lake level with wetlands during the middle Holocene (*Right*).

Table S1. Radiocarbon ages (AMS) from Laguna Blanca core A-99 and Laguna Brava core A-97

Lake	Lab code	Drive	Drive depth, cm	Composite depth, cm	Material	^{14}C age	Calibrated age range, 1σ*
Blanca	CURL-4973	1	64.5	64.5	Wood	130 ± 35	−2–−1
							14–38
							64–118
							124–147
							189–193
							213–231
							243–268
Blanca	CURL-4974	2	13.5	103.5	Leaf	660 ± 35	564–589
							641–666
Blanca	CAMS-73134	2	33.5	123.5	Wood	980 ± 40	799–813
							826–866
							901–934
Blanca	CAMS-96801†	2	85	175.0	Wood	2,700 ± 60	2,757–2,849
Blanca	CAMS-96802	3	11	188.6	Wood	2,120 ± 35	2,044–2,147
Blanca	CAMS-96803	3	90	271.7	Wood	3,480 ± 40	3,698–3,734
							3,741–3,777
							3,789–3,827
Blanca	CAMS-96804	4	21.5	310.7	Wood	4,200 ± 35	4,652–4,669
							4,704–4,757
							4,809–4,836
Blanca	CAMS-96805	5	30.25	400.3	Wood	7,055 ± 40	7,850–7,907
							7,914–7,938
Blanca	CURL-4975	6	12	419.9	Wood	7,370 ± 45	8,060–8,087
							8,159–8,216
							8,242–8,304
Blanca	CAMS-96806	6	23.5	431.3	Wood	7,550 ± 45	8,344–8,403
Blanca	CAMS-96807	6	38	445.6	Bulk	8,430 ± 50	9,429–9,502
							9,508–9,517
Blanca	UCI-23056	7	17.5	476.0	Bulk	9,430 ± 40	10,589–10,630
							10,646–10,708
Brava‡	OS-18091	5	34	862	Wood	7,610 ± 50	8,375–8,445

*Based upon the intcal04 accessed at calib.qub.ac.uk on 4/20/2006.
†Not included in age model.
‡Sample from directly above desiccation layer in Laguna Brava.